Chapter 3

Complex Langevin dynamics of spherical dimers

3.1 Overview

Often in calculation of optical forces and scattering the choice of target particle is often either a single sphere or a large agglomeration of spheres. In optical tweezing research the target particle is not guaranteed to be a sphere, instead either being an asymmetrical shape, or being a collection of smaller spheres.

As an example, while working with dense colloidal suspensions, one often ends up trapping more than one sphere. Li and Arlt [**Li2008**] studied the case of two microspheres trapped in a single OT and found that multiple trapped beads could be mistaken for a single trapped bead with an altered trap stiffness (see **??**). Theoretical studies on the case of two trapped microspheres by Xu *et al.* [**Xu2005**] employed a ray-optics based model to show that the two trapped beads are brought into physical contact with each other by optical forces and they also calculated the axial equilibrium positions of the two trapped beads as a function of their size. Experiments in [**Praveen2016**] confirmed that the two trapped beads indeed experience different trap stiffnesses in the vicinity of the same potential well.

There are further discussions looking into the dynamics of a whole host of asym-

metrically shaped particles (e.g. ellipsoids, cylinders, amorphous solids, disks, etc) [**Loudet2014**, **ShengHua2005**, **Chetana2022**], their results all showing that predicting the behaviour an arbitrary shaped particle comes with great difficulty due to the fact that the optical force is dependent on a greater number of variables such as orientation and size factors. While these have been noted as important factors, there has not been a concentrated effort to discuss their impact over the course of a typical trajectory.

With the initial goal of the project being to induce nucleation events via a rotating sphere, the aim of this chapter is to - in a limited capacity simulate and investigate the influence of a second particle being bound to our target sphere. The choice of a dimer, instead of an amorphous solid that might better represent a growing crystalline solid, allows us to consider how the dynamics of the aggregate change by varying a single parameter, namely the size ratio of the two spheres. Additionally, attempting to simulate an amorphous aggregate is rather difficult as calculating the optical force and torque is computationally slow.

In this chapter we will consider how the addition of a second sphere changes the trapping dynamics by introducing multiple equilibrium positions. In addition we demonstrate that the angular dependency of the optical force allows for multiple equilibrium orientations for a single particle. Furthermore, we look at how dimers interact with circularly polarised light, noting how our current understanding of light and particle interactions does not accurately explain the observed behaviour. We show that a dimer can undergo gyroscopic precession by utilising this unique interaction with circularly polarised light.

3.2 Simulation Details

3.2.1 Set up

As a paradigmatic example, consider a dimer suspended in water ($n_p = 1.59$) located at the focus of a Gaussian beam. The dimer is composed of two spheres with radii a_I and a_{II}, the size ratio between the two is given as a_{II}/a_I - unless stated otherwise we

kept a_I fixed at 1 μm.

The beam is focused by a objective with numerical aperture of 1.2. The polarisation is defined using the Jones vector which describes the magnitude of the x and y components of the electric field (so the vector $[1.0, 0.0i]$ describes an electric field that only oscillates in the x direction). Unless stated otherwise the Jones vector is kept at $[1.0, 0.0i]$. The conditions of the water are given as - $T = 298K,\ \eta = 1.0x10^{-3} Pa\ s,\ n_m = 1.33$.

3.2.2 Coordinate system

Throughout this project we use the work of Vigilante [**Vigilante2020**] to perform a systematic study of the dynamics demonstrated by asymmetric dimers in both plane and circularly polarised light. The simulations have two primary frames of reference that require explanation. Firstly, there is the laboratory frame which describes the coordinate system, we define the origin of our simulation as the focus of our trapping beam. While the choice in direction for the x and y axis are arbitrary the z axis is specifically chosen so that it is aligned with the direction of beam propagation.

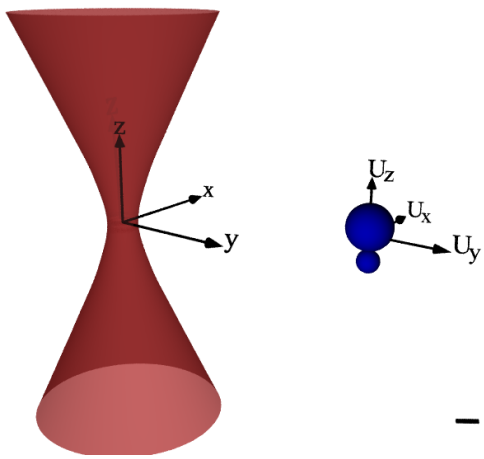

Figure 3.1: Ray scattering render of both the laboratory frame and particle frame for a dimer and a Gaussian beam. The origin of the laboratory frame is defined as the focus of the trapping beam, with the positive z-axis being aligned with the direction of beam propagation. The particle frame is centred on the dimer's centre of mass with the primary axis U_z being aligned with the centres of the two spheres. Black line is scaled to represent 1 μm.

Secondly there is the particle frame which describes the orientation state of the particle, orientations are reported as quaternions which can be readily transformed into rotation matrices. The dimer's orientation is given by a rotation matrix in the form:

$$\begin{pmatrix} U_{1,x} & U_{2,x} & U_{3,x} \\ U_{1,y} & U_{2,y} & U_{3,y} \\ U_{1,z} & U_{2,z} & U_{3,z} \end{pmatrix} \tag{3.1}$$

The matrix describes the direction of the particles 3 orientation axis U_1, U_2, and U_3. The latter is oriented so that it is collinear with the centres of the two spheres; the direction of vector U_3 is such that it goes from the centre of a_{II} to the centre of a_I. The origin of the 3 axis' is set on the particle's centre of mass, this is also used to define it's displacement from the origin of the laboratory frame.

Where U_3 represents the orientation vector that passes through the centres of both sphere's (see **??** for a full breakdown), U_1, and U_2 are orthogonal to U_3 but have no physical representation for a dimer. We can represent U_3 by it's spherical coordinates (θ and ϕ), where θ is the angle between the orientation vector and the direction of propagation and ϕ as the angle between the orientation vector and the x-axis. We define the 'standard' orientation as being aligned with the direction of beam propagation direction ($\theta = 0°$) - and therefore the 'inverted' orientation is defined when the dimer is orientated against the direction of beam orientation ($\theta = 180°$) - see fig 3.2 for a visual of the laboratory and particle frame.

3.2.3 Diffusion Matrix

In order to compute the magnitude of the Brownian forces we need to know the dimer's diffusion matrix **D**. Unlike for spheres where the translational and rotational diffusion coefficients are equal along all three Cartesian axis', a dimer's translational and rotational diffusion is dependent on whether we consider the its long or short axis. We use the results from [**Nir1973**] to compute the dimensionless diffusion matrix and then scale it according to the radius of the largest sphere (a_I). The dimer's centre of diffu-

sion is located a distance of $a_I\zeta$ from the point of contact between the two spheres, the coefficient ζ is based on the size ratio of the two spheres. We use the centre of diffusion as the target origin that is provided to *mstm*

3.2.4 Equations of Motion

The main equation of motion for an optically trapped particle is the Langevin equation. For a dimer the equation remains the same but is altered slightly to account for coupling between rotational and translational motion.

$$\frac{d\vec{r}(t)}{dt} = \frac{\vec{\kappa}_x}{\gamma}\vec{r}(t) + \sqrt{2\vec{D}_x}\eta(t) \tag{3.2}$$

Where $x(t)$ is replaced with $\vec{r}(t)$ to signify that the translational motion is generalised to a 3 dimensional case. Here we omit the inertial term as the restoration time of the optical trap is far greater than the characteristic time of the particle ($\kappa/\gamma \gg m/\gamma$). Now, the dimer is undergoing random rotational motion in addition to its Brownian translational motion the first term on the right hand side is no longer purely a function of the dimer's position but also of its orientation. The rotational form of the Langevin equation for a dipole within an external potential is given as [**Mazo2008**]:

$$\frac{d\vec{u}(t)}{dt} = \frac{\mu}{\gamma_R}\left[\vec{u}(t) \times E(t)\right] \times \vec{u}(t) + \sqrt{2k_BT\vec{D}_R}\lambda(t) \times \vec{u}(t) \tag{3.3}$$

Where $\vec{u}(t)$ is the unit vector aligned along the centres of the two spheres, μ is its dipole moment, and γ_R is the rotational friction coefficient which is given as $\gamma_R = 8\pi\eta r^3$ for a sphere. The term $E(t)$ corresponds to the time dependent electric field vector, however we can assume that over a time step as large as ours the time variation in the electric field is so insignificant that it can be treated as a constant. If we assume that over the course of a trajectory the dimer has a 'equilibrium' orientation in which the optical torque is minimised we can say that the first right hand term can be replaced with $\vec{\kappa}_u(\vec{r}(t))$ to represent a harmonic potential due to the torque. $\lambda(t)$ is the Brownian rotations from the surrounding fluid, like in the translational case the Brownian torque

are normally distributed and are also uncorrelated so that:

$$\langle \lambda(t)\lambda(t') \rangle = \delta_{ij}\delta(t-t') \tag{3.4}$$

For an asymmetric scatterer whose radius is comparable to that of the electric field's wavelength we now have a system of simultaneous equations:

$$\frac{d\vec{r}(t)}{dt} = \frac{\vec{\kappa}_x(\vec{u}(t))}{\gamma}\vec{r}(t) + \sqrt{2k_BT\vec{D}}\eta(t) \tag{3.5}$$

$$\frac{d\vec{u}(t)}{dt} = \frac{\vec{\kappa}_u(\vec{r}(t))}{\gamma_R} \times \vec{u}(t) + \sqrt{2k_BT\vec{D}_R}\lambda(t) \times \vec{u}(t) \tag{3.6}$$

Fortunately, we do not need to solve these directly as the latter two random variables can be easily approximated if the thermal energy of the system is known, and the rate of change can be assumed as linear if we take a sufficiently small time step that $\Delta t \ll \kappa_x/\gamma$ & $\Delta t \ll \kappa_u/\gamma_R$. In doing so we now only need to compute the optical force and torque applied to the dimer.

3.2.5 Computational methods

Using a MATLAB package called *Optical Tweezer Toolbox* or *ott* [**Nieminen2007**] we can compute the beam shape coefficients (a_{nm} & b_{nm}) for any desired beam type. Using the results from [**Farsund1996**] we can then compute both the optical force and torque using the beam coefficients and the scattering coefficients (q_{nm} & p_{nm}) which are found by calculating the dimer's T-matrix via *mstm* [**Mackowski2011**] and then using (**??**). The total force in along the z-direction and the total torque about the z-axis are provided:

$$\begin{aligned}\mathbf{F_z} = -\frac{1}{4\pi k^2}\sum_{n,m}\Bigg(&\frac{m}{n(n+1)}\Im[a_{nm}b^*_{nm} - p_{nm}q^*_{nm}] \\ &+ \frac{1}{n+1}\left[\frac{n(n+2)(n-m+1)(n+m+1)}{(2n+1)(2n+3)}\right]^{1/2} \\ &\times\Im[b_{nm}b^*_{nm} + a_{nm}a^*_{n+1m} - q_{nm}q^*_{nm} + p_{nm}p^*_{n+1m}]\Big)\end{aligned} \tag{3.7}$$

$$\begin{aligned}\mathbf{T_z} = -\frac{1}{8\pi k^3}\sum_{n,m}\Bigg(&\frac{m}{n(n+1)}[|a_{nm}|^2 + |b_{nm}|^2 - |p_{nm}|^2 - |q_{nm}|^2] \\ &+ \frac{2}{n+1}\left[\frac{n(n+2)(n-m+1)(n+m+1)}{(2n+1)(2n+3)}\right]^{1/2} \\ &\times\Re[b_{nm}a^*_{nm} + a_{nm}b^*_{n+1m} - p_{nm}q^*_{nm} + q_{nm}p^*_{n+1m}]\Bigg)\end{aligned} \tag{3.8}$$

where a_{nm}, b_{nm}, p_{nm}, and q_{nm} are the beam coefficients of the incident and scattered fields respectively. We can get the x and y force and torque components in a similar form by applying a simple rotation transformation. With the optical forces and torques computed all that remains is to compute the Brownian forces and torques which are constrained by the relation.

$$\langle q_i q_j \rangle = 2D_{ij}\Delta t \tag{3.9}$$

Vigilante et al compiled together a python package that combines both *ott* and *mstm* to simulate the behaviour of spherical aggregates within a predefined optical trap [**Vigilante2020**]. Now *ott* does have inbuilt T-matrix modules that can be used to model the scattering from different shaped particles; however, for aggregates of spheres the resultant force is nonsensical (see Chapter 4 for further details). As such we rely on the *mstm* for simulating dimers.

3.3 Positional and Orientational dependence of Trapping forces

First, let us look at how the addition of a second sphere changes how we go about looking for equilibrium positions relative to the beam focus. Typically when trapping a target particle we do not care where it is spacially in relation to the trap focus, we assume that it will end up in the same equilibrium position regardless. This assumption can not be taken when considering a dimer, or any aggregate of spheres.

If we wanted to start from first principles and determine the trap strength on our target particle the first step would be to locate the equilibrium position relative to the trap focus. For a single sphere it is easy to enough to understand that its centre of

mass will be drawn to focal point of the laser due to gradient forces, once there the force is analogous to a harmonic spring with a fixed trap stiffness (see fig.**??**). Now, if we consider instead a dimer, we now have two spheres both being drawn to the focus along by the same gradient force; in addition the scattering force is significantly more complex due to both spheres scattering the electromagnetic fields. This mutual scattering between individual spheres is what makes simulating spherical aggregates far more difficult compared to a single sphere, and even harder still to predict the position where the dimer's centre of mass is in equilibrium.

Because the scattering force is only significant in the direction of beam propagation [**Capitanio2002**] we can assume there will only be a single potential well lying at the centre of the beam. Along the beam axis, such an assumption is no longer valid due to fact that spherical aggregates experience inter-particle scattering. This is a key reason for using *mstm* as it accounts for that behaviour. The methodology for computing optical forces has been covered extensively for a number of different trapping conditions [**RanhaNeves2019**]. So it is relatively easy to compute the trapping force and determine the equilibrium position by finding the position that minimises the net optical force and the local gradient is negative ($\delta F/\delta x < 0$) - we can assume that for a dielectric sphere the optical torque is negligible. For a dimer (or any arbitrary spherical aggregate), we now must consider both its position and orientation and find where the net optical force and torque are minimised.

After computing its T-matrix via *mstm* and supplying that to *ott* we compute the optical force exerted by a 50 mW laser via (3.7) in the axial direction while the dimer is in its 'standard' orientation. As expected we see a single point where the dimer will be in equilibrium, the linear fit in fig. 3.2(a) indicates a that the force can be modelled as a harmonic potential close to the equilibrium position ($F_z \approx -\kappa_z z$). The second point where the axial force goes to 0 cannot be considered as equilibrium position as the positive gradient indicates that the trap is unstable unless Brownian motion is ignored.

We repeated the same calculation but now while the dimer is in its 'inverted' orientation, instead of a single point where the optical force is minimised we see that there are instead two separate equilibrium positions, one above the focus and one below the

focus. In this particular example the two positions are far enough apart that both can be considered as separate harmonic traps.

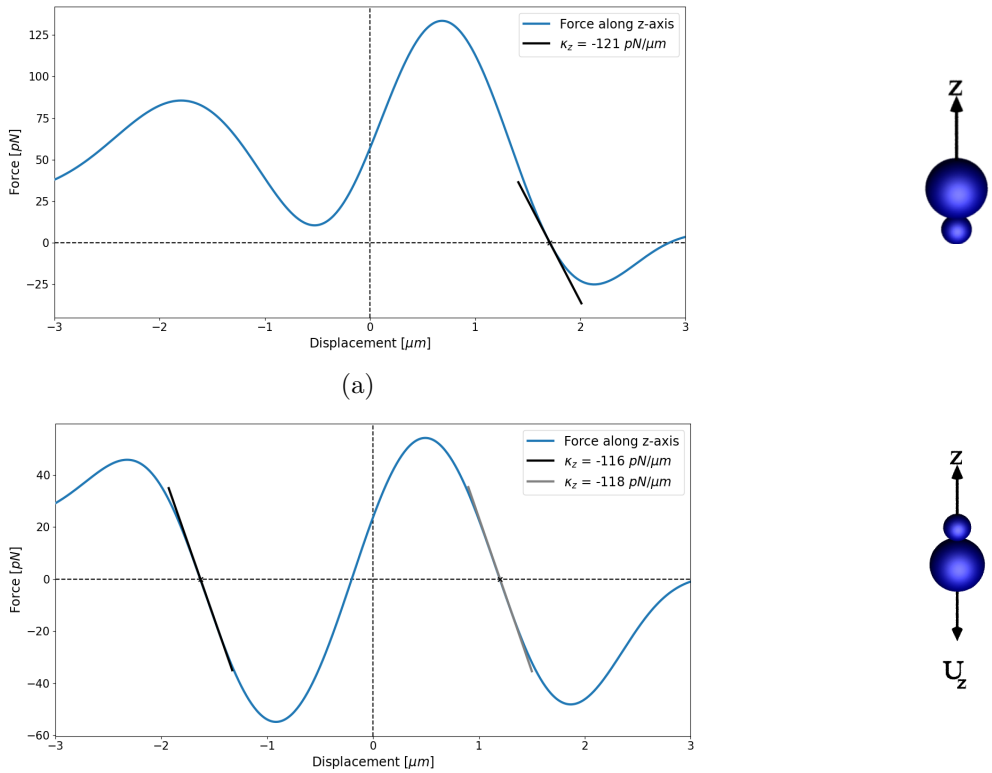

(a)

(b)

Figure 3.2: Plots of force vs displacement of the centre of mass of the dimer (µm) for the case of a dimer of size ratio 2. (a) is the case where the dimer is in its' 'standard' orientation, where the dimer is trapped at $z = 1.71\ \mu m$. (b) is the case where the dimer is in its' 'inverted' orientation, the dimer is trapped at two positions: $z = 1.20\ \mu m$ & $z = -1.63\ \mu m$. On the left are renders to visualise the dimer orientation are shown below each plot. The black lines on each force-curve is a linear fit with the slope being reported as the trap stiffness in the legend.

This is different to a single sphere, namely in that a single sphere should only have one equilibrium position and that it is much closer to the trap focus ($\approx 0.05\mu\ m$ from the focus). This is also not similar to other works where random clusters of spheres have been shown to oscillate between stable points [**Vigilante2020**].

We can see that both equilibrium positions have comparable axial trap stiffness (κ_z), however the difference in the transverse trap stiffness (κ_x) is far more noticeable. The

same dimer was trapped at each of the axial equilibrium positions and the transverse force was evaluated. While in all three cases the dimer can be trapped the linear range where that would typically associated with a stable trap is far narrower in the 'standard' orientation compared to the 'inverted' cases. This highlights one of the challenges involved with studying asymmetric particles, even though its a simple enough process to trap them they maybe characterised very differently depending on their relative position and orientation towards the focus. This can have a significant impact on rheological studies - or attempting to probe any local property - as the variance in trap strength can result in large errors over repeated measurements.

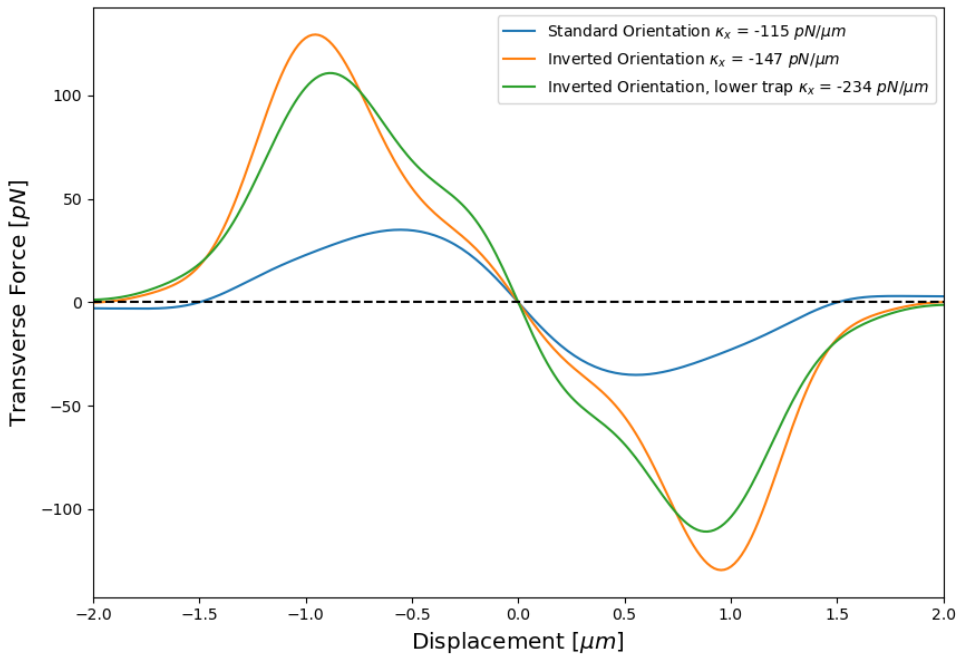

Figure 3.3: Plots of force vs displacement of the dimer's centre of mass spheres, where a positive force indicates the dimer is directed right on the x-axis, and vice versa for a negative force. The same simulation parameters are used here as in fig 3.2 (a) and (c). The blue curve representing the force response for a dimer in its standard orientation, orange being the inverted case, and green the same case but placed below the focus.

For completeness the harmonic traps were located for dimers across a range of size ratios - from $a_I/a_{II} = 1$ to $a_I/a_{II} = 10$ - while also recording the trap stiffness for each trap. The same simulation parameters are used here as for figures 3.2 & 3.3. As shown in Fig. 3.4 a_{II} decrease the dimer begins to approximate a single homogenous sphere - at least in terms of location and trap strength. However, for intermediate sized dimers (between $a_I/a_{II} = 1.1$ to $a_I/a_{II} = 4$), a second equilibrium position is found below the trapping focus. We should note that there are also unstable traps that exist, these are also depicted in fig. 3.4. While the optical force is zero at these positions the gradient $\delta F_z/\delta z$ is positive and so any Brownian motion would displace the dimer, either ejecting it from the optical trap or letting it be drawn towards another harmonic trap.

Previous work using the ray-optics model have confirmed even in the case that two spheres begin separated the electric field will align the particles as such that they make contact and are trapped together about a single trapping position [**Xu2005**]. Furthermore it has been shown through proper manipulation of the Gaussian or Bessel beam modes that any number of trapping potentials can be developed [**Shahabadi2020**] for nanoparticles. This result however, is the first example of an orientation dependent trapping situation using only a TEM_00 beam. Typical experimental arrangements cannot determine much information on the axial position of a trapped particle relative to the trap focus; this result indicates not only that dimers can be trapped in multiple axial positions but also their trapping behaviour is heavily dependent on the axial position. As such it is necessary that positional information in the z-axis can be elucidated if multiple spheres are trapped simultaneously.

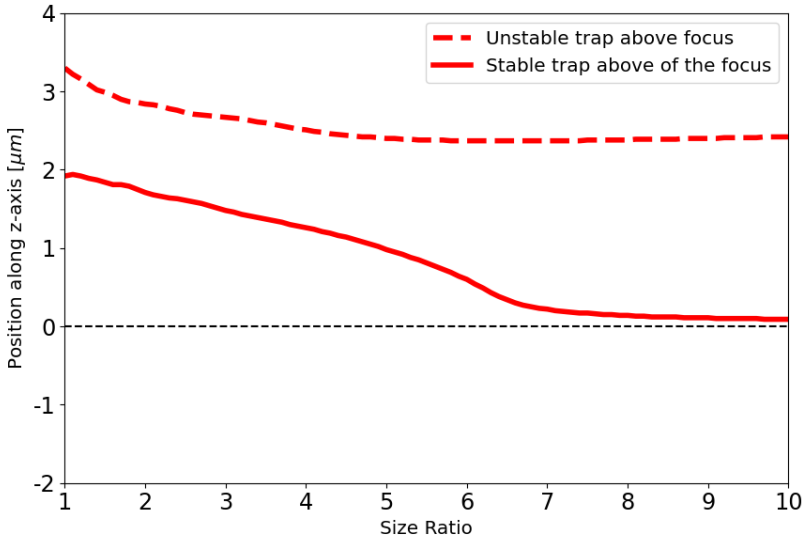

(a)

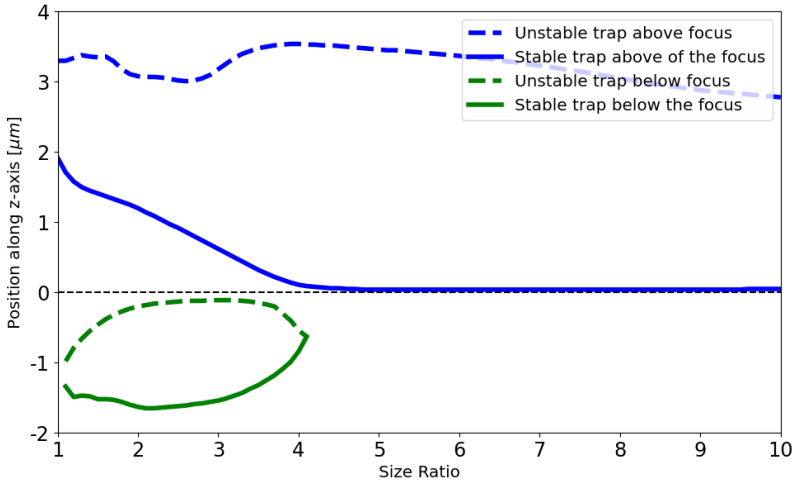

(b)

Figure 3.4: Equilibrium positions of optically trapped dimers with varying size ratio, dashed lines represent unstable traps whereas solid lines are for stable equilibrium positions. (a) shows that dimers while in their 'standard' orientation will always have a single equilibrium position. (b) shows that when the same dimer is in its' 'inverted' orientation can be trapped in two axial positions, one below the focus and one above the focus.

3.4 Non-trivial basins of attraction

As mentioned previously in **??** the torque applied to an anisotropic scatterer can be broken down into two categories: torque generated from the field polarisation and torque generated by the gradient force of the electric field. The former is generally only applicable for objects that are birefringent whereas the latter is applicable to dimers due to their elongated shape. Since both spheres are attracted towards the centre of intensity via the gradient force a dimer will experience a restoring torque that keeps the it in an equilibrium orientation. For any elongated particle the torque is minimised when the long axis is aligned either parallel or perpendicular with the direction of the electric field. In this section we try to find equilibrium configurations (positions and orientations where both the optical force and torque are minimised).

Computing the equilibrium positions when a dimer is aligned with the electric field is relatively simple as the orientational torque is minimised (see Eq. **??**). Meaning once trapped the dimer is unlikely to change orientation enough to escape the trap. Regardless, that does not rule out the possibility that there is a stable configuration where the orientation not strictly vertical, in fact most experimental work with symmetric nano-dimers will trap them lying perpendicular to the beam direction [**Ahn2018**, **Reimann2018**]. Unlike in Sec. 3.3 we cannot simply compute the optical force and torque as the parameter space is too large and determining if a particular position and orientation is stable is not clear based solely on force and torque measurements [**Bui2017**]. Using the same simulation parameters as before we ran a number short simulations (total simulation time was 0.005 s) with the laser power increased to 500 mW. Each simulation started with the dimer in a different starting position and orientation, due to the high laser power the dimers either escaped the trap or were stably trapped. We chose to only consider the $z-\theta$ phase space in order to simplify the explanation, considering all possible parameters would increase the simulation time significantly. The $z-\theta$ phase space can be divided into different regions depending on which equilibrium configuration is reached.

Where the each starting location is colour coded to match the final equilibrium

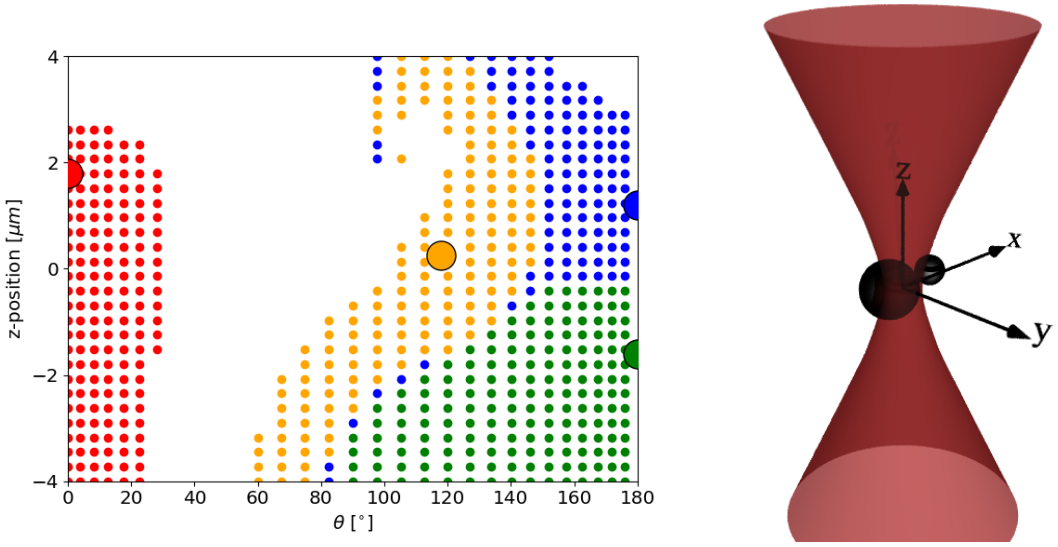

Figure 3.5: Map of $z - \theta$ phase space using a dimer of size ratio 2 with a laser power of 500 mW ($\theta = 0°$ is the 'standard' orientation and $\theta = 180°$ is the 'inverted' orientation). The stable configurations are indicated by the larger circles and the starting conditions are colour coded to match the stable point they end up in. Right hand render shows a dimer in its off-axis configuration.

position reached, empty regions indicate that the trap was escaped. As expected we see that the dimer has three separate traps when the dimer is close to its vertical orientation, similar to what we see from figs. 3.2 and 3.4. When the beginning orientation is close to horizontal there exists a 4th harmonic trap. Each of these traps, has its own 'basin' of attraction around which the dimer is drawn into, the strange shape of these basins is likely due to how the asymmetric shape interacts with the optical trap.

Interestingly while the trap strength of these off-axis configurations are similar in magnitude to the vertically aligned dimers, but when the laser power is lowered (around 5 mW) the traps appear metastable. With the vertical configurations even after 30 s of simulation time the dimer is still trapped whereas the off-axis configuration can be escaped after only a few seconds of simulation time. The suggested that the configuration is metastable is due to the increased rotational freedom. Similar configurations have been explored with ellipsoids; Zhu *et al.* looked at the dynamics of various elliptical particles and found that regardless of shape or initial orientation the particle

would tend towards either a purely vertical or purely horizontal orientation [**Zhu2021**]. However, in our case the dimer never returns to a vertical orientation, suggesting their is a potential barrier separating the different configurations. In order to build a better understanding of the potential landscape we need to consider how the force and torque vary for a dimer in the $z - \theta$ phase space.

3.4.1 Force-Torque landscape of an arbitrary dimer

We use *ott* to compute the optical force and torque for the same dimer as used in fig. 3.5 in different positions or orientations, this is depicted in fig.3.6.

The optical torques reported by *ott* are about their respective axis - so T_x is the torque that rotates the dimer about the x-axis in the particle frame.

The magnitude of the force and torque are indicated by the colour intensity, with white indicating either zero force or torque. This helps show where a dimer may end up in equilibrium by finding where both the torque and force go to 0.

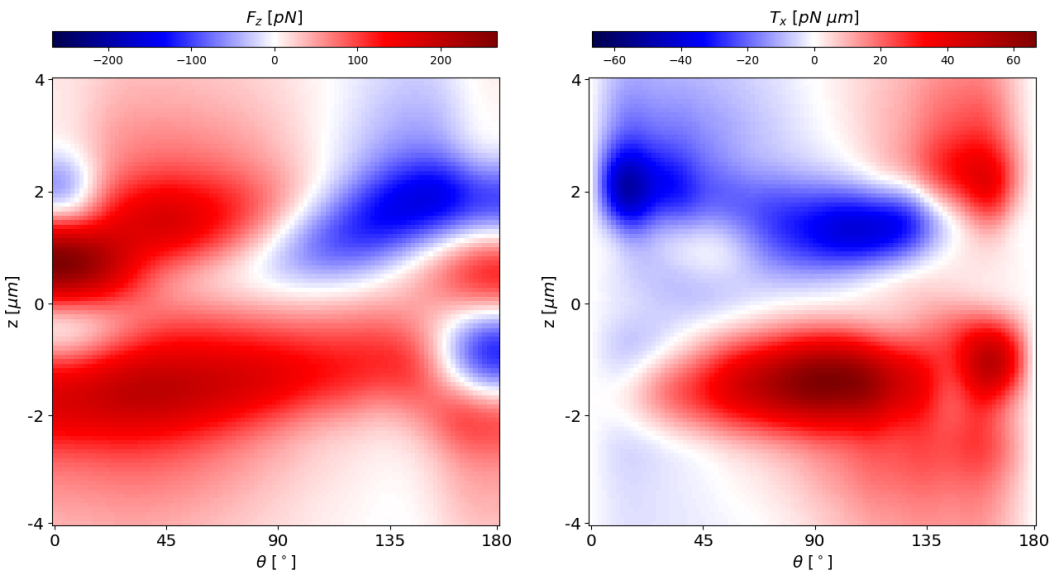

Figure 3.6: Force-Torque landscape over the $z - \theta$ phase space with a dimer is a size ratio of 2, laser power of 100mW. Left: 2D plot of the optical force in the axial direction as a function of position and orientation. Right: 2D plot of the optical torque about the x-axis as a function of position and orientation.

The force and torque landscape provides some insight into how the dimer can inhabit

an off axis equilibrium orientation. Firstly, lets consider a typical trap, while the dimer is close to vertical; in all of these cases the optical force and torque directs the dimer back to the configuration. In this case the potential well is positive whether the dimer moves along the z-axis or is rotated. We can assume that in both cases the translational and rotational stiffnesses are close enough to be modelled as harmonic potentials.

However when in an off-axis configuration ($z \approx 0$ & $90° \leq \theta \leq 115°$) the optical torque is working against the optical force, trying to move it out of equilibrium while the optical force returns it to equilibrium. This means that the potential well is more akin to a saddle point, the only reason that the optical trap is not escaped immediately is because the the translational trap stiffness is significantly greater than the gradient of the optical torque ($\kappa_z \gg \kappa_\theta$). Therefore it is more accurate to say that the trap is not metastable, as when the trap is escaped it is not because the Brownian displacement is greater than the potential well, rather the dimer is randomly traversing along the x-axis (aka random Brownian rotation) and has escaped the translational potential well.

The force-torque landscape also provides an explanation to the boundaries between the different trapping 'basins' in fig. 3.5. The first point of interest is the 'dead zone' around the orange basin. Looking at fig. 3.6 we can see that around that region ($z \approx 2.5\mu$ & $\theta \approx 110°$) the optical torque changes sign as you move closer to the trap focus. There is no clear physical reason why the optical torque change direction so abruptly but a consequence of it is that dimers that are too close to this region of the torque landscape are ejected from the optical trap as the are drawn down towards the trap focus.

The only pellicular result is the observation that the blue basin can still be reached well below the trap focus. As shown by fig. 3.5 there are a handful of starting configurations that end up in the upper trap while in the inverted orientation. Even consulting fig. 3.6 does not indicate any reason why this occurs. The only conclusion we can draw is that the orange and green basins of attraction are small enough that it is possible for a dimer to avoid both.

3.5 Continuous rotational motion in circularly polarised light

One aspect that has yet to be covered in depth with regards to spherical aggregates of any construction is their interaction with circularly polarised light. For homogenous spheres the optical torque is regarded as being negligible as the spin density cannot impart angular momentum while propagating in a homogenous medium. Dimers however, have been shown to experience an optical torque [**Vigilante2020**, **Ahn2018**, **Reimann2018**] while trapped in a circular polarised beam. In our simulations we found that dimers would rotate about their long axis when trapped in circularly polarised light. In this section we want to discuss how this behaviour is influenced by size, position, and orientation; and furthermore, we wish to address possible explanations for this behaviour, as none of the current theories into optically induced rotation seem plausible.

3.5.1 Polarisation Dependency on Dimer trajectory

In their paper Vigilante *et al* attribute the rotational motion to the anisotropic shape of the dimer [**Vigilante2020**]. Anisotropic scattering is a viable theory for describing optical rotation, however there is usually an optical axis about which rotation occurs. For a dimer this is typically the orientation vector that passes through the centres of both spheres [**Ahn2018**, **Reimann2018**, **Bruce2020**]. There have been cases where the particle's cross sectional shape is engineered to scatter light in one particular direction [**Higurashi1994**], but if this was the case then the dimer should rotate when illuminated by any polarisation of light.

To that end, we simulated the motion of an optically trapped dimer in beams of varying polarisation ($NA = 1.2$, $P = 100\ mW$). As mentioned previously the beam polarisation is given using the Jones vector, for each simulation we vary the phase in increments of $\pi/24$.

Each simulation was run for 1 second ($\Delta t = 10^{-5}\ s$) and at the end we looked at the orientational time series; the dimer's orientation is recorded as a quaternion which

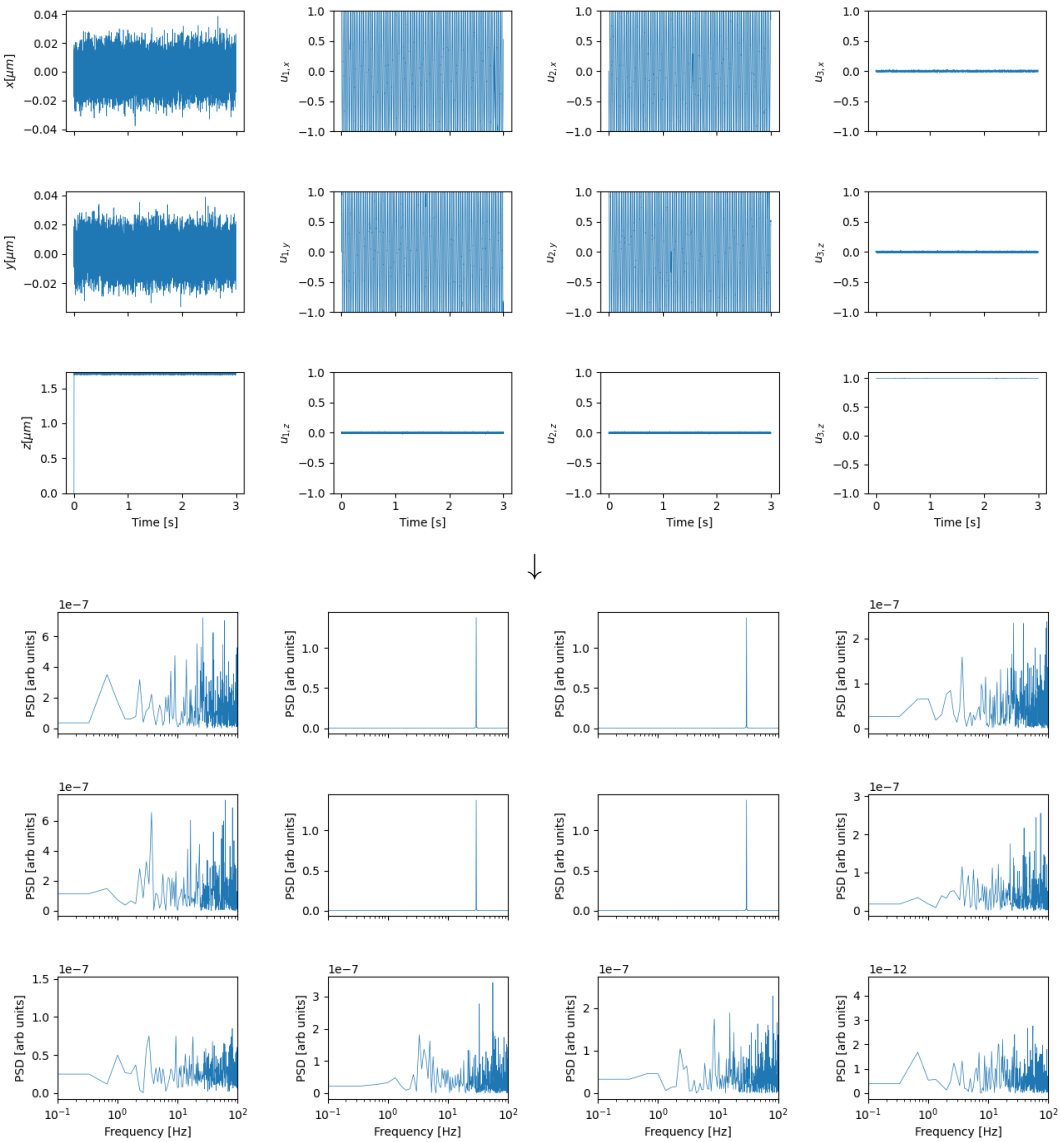

Figure 3.7: Top: 3 second trajectory of a dimer trapped by a circularly polarised Gaussian beam. The far left column depicts the dimer's centre of mass position with time; the remaining 3 columns show the 9 components of the dimers' rotation matrix, with each column being associated with one of its three principal axis. Bottom: The same trajectory but each time series has been replaced with its Fourier transform. The only non-zero elements are for the $U_{1,x}$, $U_{1,y}$, $U_{2,x}$, and $U_{2,y}$ which show a single peak at the rotation frequency.

can be easily converted to a 3-dimensional rotation matrix. By considering only the transverse components ($U_{1,x}$, $U_{1,y}$, $U_{2,x}$, & $U_{2,y}$) of the rotation matrix and taking the

Fourier transformation of their time series reveals the rotational frequency. The laser power is set to 100 mW to avoid large thermal fluctuations and so that the Fourier series of the transverse components approximates $\delta(\omega_{rot} - f)$ - the Dirac delta function centred at the rotational frequency ω_{rot}. This is demonstrated in fig. 3.7

If the rotational frequency was not immediately obvious the simulation was repeated but over a longer simulation time. Four different size ratio of dimers were studied, both in their 'standard' and 'inverted' orientations. The results of this are displayed in Fig. 3.8:

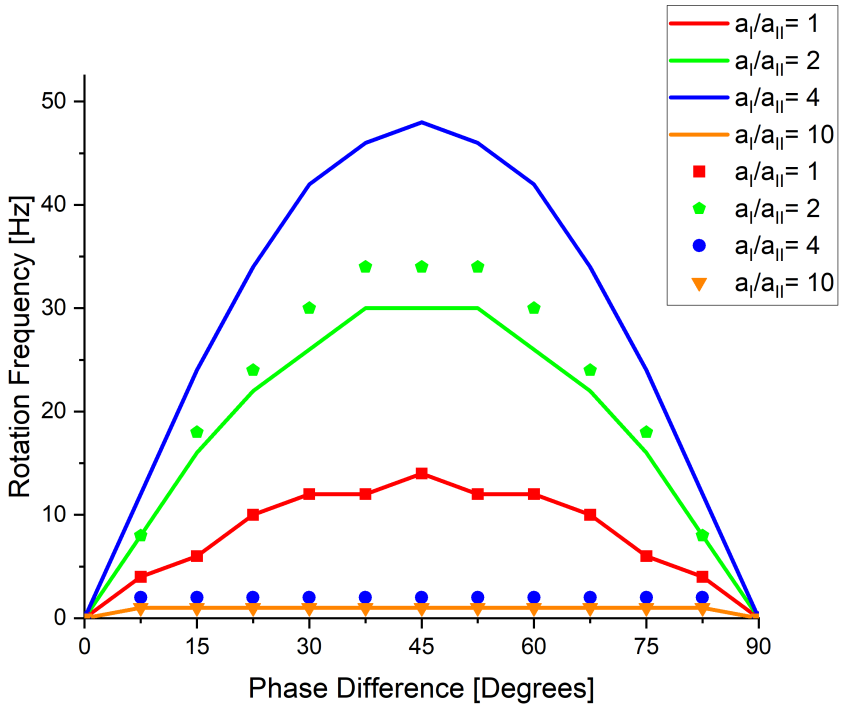

Figure 3.8: Rotation frequency vs electric field phase difference for differently sized dimers. The solid lines represent the rotation rate experienced while the dimer is in its standard orientation, whereas the solid points are for the case where the orientation is inverted. Laser power = 100 mW.

This shows us that these optical rotations are polarisation dependent and not merely an example of the dimer scattering light asymmetrically. We also know that this cannot be a similar mechanism to that of experimental works [**Ahn2018**, **Reimann2018**] as in our simulations the dimer's long axis is parallel to the electric field. In this orientation

the dimer's optical axis is aligned perpendicular to the polarisation vector meaning that there should be no angular momentum transferred along the optical axis. This is consistent with other experiments involving elongated particles. A dual beam trap was used to study the dynamics of "disk like" particles. They found that these particles had one of two stable orientations: Either orienting with the 'flat' side perpendicular to the beam trap, with no rotation being observed [**Brzobohaty2015**]. Or orientating with the 'flat' side parallel to the trap, in which case the long axis was aligned with the polarisation vector and thus rotational motion was detected [**Brzobohaty2015**].

3.5.2 Brownian Vortex via Curl of Spin momentum

In their work Vigilante refers to the spin-curl effects demonstrated by Grier *et al* [**Ruffner2012**], in which the curl of the spin density leads to a second order optical force that orbits around the beams central axis [**Yevick2017**]. While several papers have demonstrated this phenomena [**Zhao2007**, **Zhao2009**, **Wang2010**] it was only properly formalised by [**Ruffner2012**]. In which they showed that the seemingly random trajectory of a trapped sphere was biased by the polarisation state of the trapping beam. While not immediately evident from the trajectory the helicity of the trapping beam was revealed by computing the particle's probability flux using.

$$j(r) = \frac{1}{N-1} \sum_{j=1}^{N-1} \frac{r_{j+1} - r_j}{\tau} \delta_{sigma_j} \left(r - \frac{r_{j+1} + r_j}{2} \right) \tag{3.10}$$

where δ_{σ_j} is the kernel of an adaptive density estimator [**Silverman1986**]. (3.10) describes the direction a trapped sphere is most likely move in given our statistical knowledge of the trajectories probability density function. A finite estimation of the density function $p(r)$ is used in [**Ruffner2012**].

$$p(r) = \frac{1}{N} \sum_{j=1}^{N} \delta_{\sigma_j}(r - r_j) \tag{3.11}$$

The probability flux reveals a biased motion in the trajectory of a single sphere (see Fig. 3.9). This biased motion results in a slight orbital motion about the central

axis of the trapping beam, the orbital frequency is shown to be proportional to the polarisation state of the trapping beam.

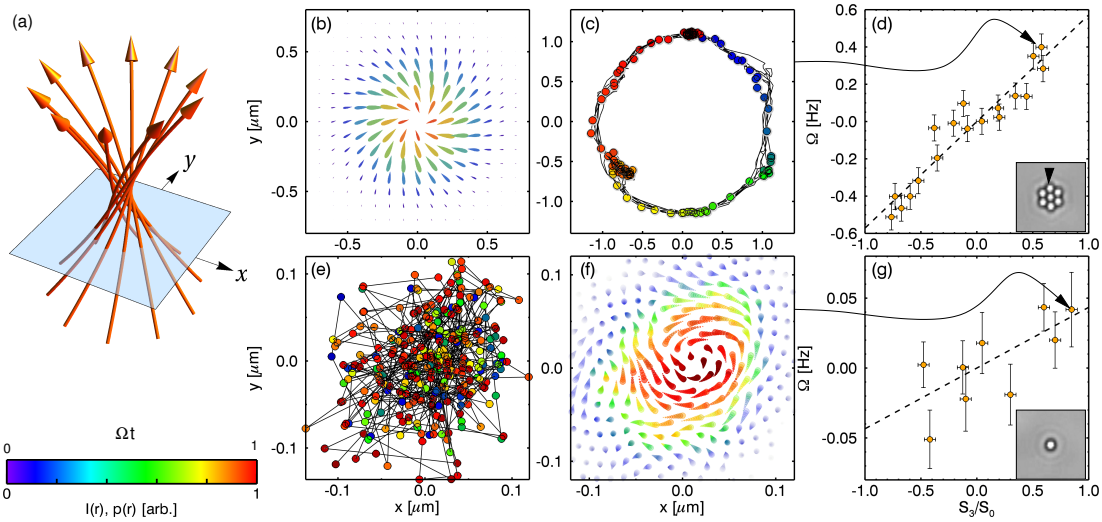

Figure 3.9: Figure reused from [**Ruffner2012**]. (a) shows how the momentum density of a Gaussian beam is twisted while using circularly polarised light. The top row (figures (b)-(d)) shows a 7 sphere cluster trapped in a circularly polarised beam. Due to the clusters asymmetric susceptibility to polarization the cluster rotates in the $x-y$ plane. Whereas the bottom row (figures (e) - (g)) show the similar results for a single sphere. In this instance the sphere does not rotate but instead orbits the beam axis. In both instances the motion is proportional to the degree of polarisation (see figures (d) and (g)) but for the single sphere this motion is only revealed when using (3.10) & (3.11). Reused with permission from author

While the results from [**Ruffner2012**] suggest that the optical rotation seen in asymmetric dimers can be attributed to the same spin-curl forces there are several questions that cannot be explained purely by the spin-curl force.

3.5.3 Optical torque differences

In their paper Grier *et al* show that a 7 sphere cluster will rotate when trapped in circularly polarised light but a homogenous sphere will have a slight curl to its trajectory. They attribute this to the curl of the spin angular momentum generating a "Brownian vortex". But what is more interesting, and something that appears unaddressed, is how the effects of this vortex change based on the overall shape of the target particle.

You would not expect that the addition of a single additional sphere should dras-

tically adjust the torque especially if said sphere is relatively small. However when we measured the optical torque of a single sphere and a dimer - $a_I/a_{II} = 10$ - we found the exact opposite. In both cases we used the same trapping beam as used for fig. 3.8 but with a circularly polarised beam. Both the sphere and dimer were rotated in the $x - z$ plane and the all three components of the optical torque were recorded.

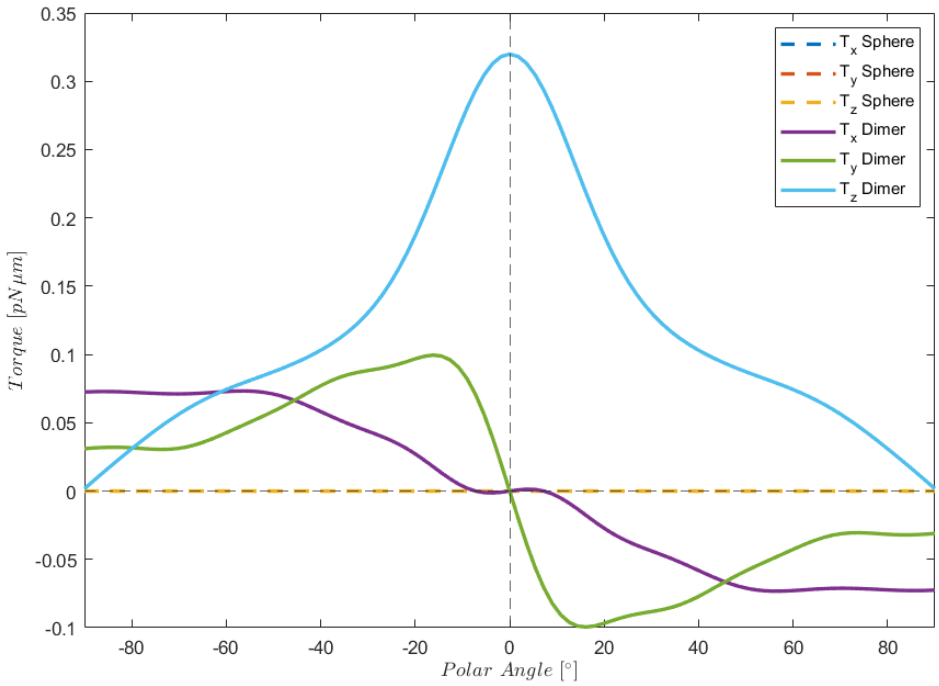

Figure 3.10: Optical toque experienced by a dimer ($a_I/a_{II} = 10$) and a single isotropic sphere. Both were rotated in the $x - z$ plane and the angle between U_z and the beam axis gives the polar angle.The solid lines denote the torque experienced by the dimer whereas the dashed lines represent the torque experienced by the sphere.

The torques about the x and y axis can be somewhat understood as the second sphere is being drawn back towards the centre of the trap by the gradient forces. The same cannot be said for the z- component of the optical torque, which is non-zero even at a 80° angle. This cannot be simply explained via spin-curl effects, as the 'Brownian vortex' should instead be driving the dimer around the beam axis - similar to how the 7 sphere cluster behaved. What is clear that the mere combination of two spheres results in a unique behaviour that has not been previously investigated.

3.5.4 Rotational frequency as a function of size ratio and orientation

One factor t Intuitively, you would expect that a larger particle would experience a greater torque and therefore rotate faster. By repeating the same kinds of simulation as used in 3.8 but for a circularly polarised beam $\phi = 90\circ$ it was found that not only is the rotation rate dependent on the size of the dimer, but also on its orientation and therefore their axial position.

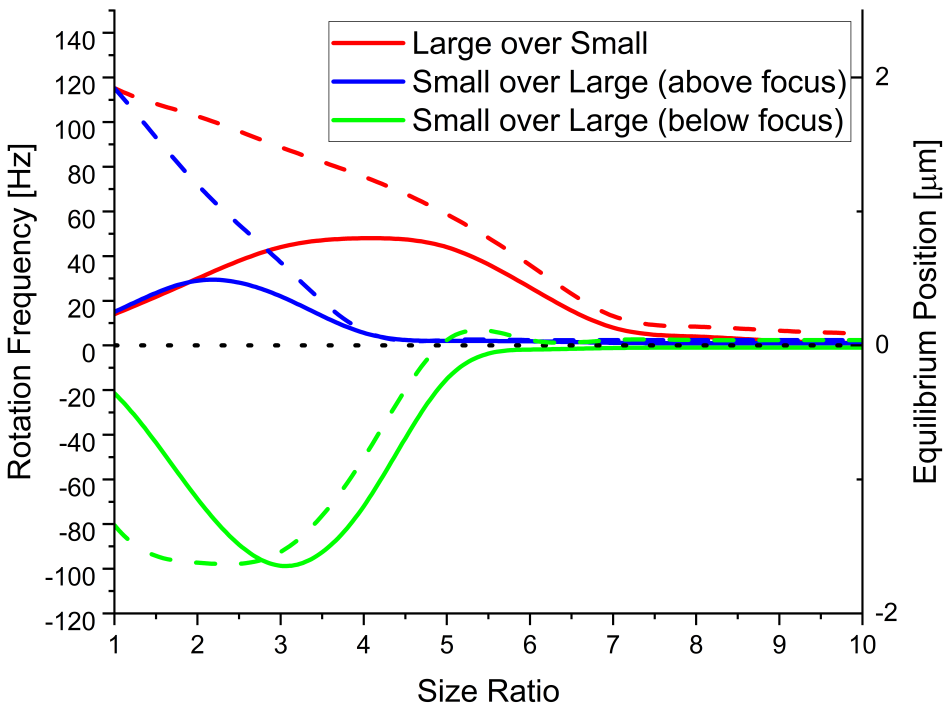

Figure 3.11: Rotation rate plotted against dimer size ratio while trapped in a circularly polarised beam; a positive rotation rate indicates clockwise rotation, whereas a negative rotation rate indicates counter-clockwise rotation. The red line is for the case of a dimer in its 'standard' orientation. The blue line is for the case when the dimer is in its 'inverted' orientation while trapped above the focus of the beam. And lastly the green line is for the case when the dimer is in its 'inverted' orientation, but when it is trapped below the focus of the beam.

It is difficult to see from the graph, but the rotation rate never truly goes down to zero, reaching a minimum of 2 Hz, which would imply that a second sphere of radius

200 nm is enough to induce rotational motion. It is not clear if the optical torque calculated for the larger size ratios is accurate as you would not expect the rotation rate to plateau like this. From fig. 3.10 it seems clear that the torque is not merely an error of the numerical calculations as it would not have such a strong angular and positional dependence. Most likely with longer simulation times would reveal the real relationship behind the rotation rate and the size ratio.

What is also interesting is that the rotation rate is not correlated directly with either the particle size or the equilibrium position. This is in stark contrast to previous reports of dimer optical rotation; Ahn *et al.* reported that the rotational frequency is maximised when the dimer is symmetric [**Ahn2018**]. Their work was conducted experimentally in a vacuum so the only limiting factor to the optical rotational motion is the structural stability of the particle itself.

3.5.5 Gyroscopic Precession using asymmetric dimers

As mentioned in section 3.4 for specificity sized dimers there is the potential for non-vertical trapping orientations in which the dimer is still stably trapped. When a circularly polarised beam is used the dimer exhibits gyroscopic precession. As shown in fig. 3.12 the dimer's trajectory exhibits periodic rotation, both around its long axis and about the beam axis.

Applying a Fourier analysis to the above trajectory reveals the 3 fundamental frequencies typically associated with gyroscopic precession. Fig. 3.13 gives a representative idea of the motion seen in fig. 3.12. Firstly there is precession, is denoted by ψ, this causes the dimer to rotate in the XY plane while maintaining a constant polar angle. The precession can be due to the dimer having inhomogeneous polarisation susceptibility. Since its long axis is more susceptible to being polarised the dimer will try to align its long axis with the polarisation vector [**Bruce2020**]. Second there is nutation, denoted by θ, which is due to the dimer's Brownian motion being influenced by the 'Brownian vortex', as predicted by [**Ruffner2012**]. And lastly there is rotation, denoted by ω, where the dimer spins around its long axis as it did in 3.5.1 & 3.5.4. If the rotation was due to the curl of the spin angular momentum then you would only

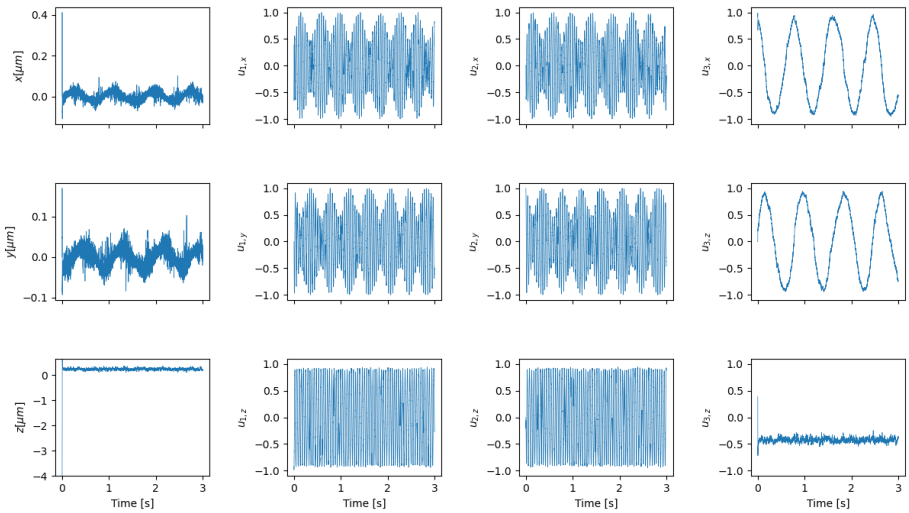

Figure 3.12: 3 second trajectory of a dimer ($a_I/a_{II} = 2$) trapped in an off axis orientation with a circularly polarised beam ($P = 100\ mW$). The far left column depicts the dimer's centre of mass position with time; the remaining 3 columns show the 9 components of the dimers' rotation matrix, with each column being associated with one of its three principal axis.

expect to see precession and nutation, the addition of rotational motion suggests that having multiple particles in close proximity results in a transfer of angular momentum along the long axis.

What is interesting is that while we see the precession and nutation also contribute to the rotation frequency. As can be seen in both fig. 3.12 and fig. 3.13 the rotation matrix components $U_{x,x}$, $U_{x,y}$, $U_{y,x}$ and $U_{y,y}$

This gyroscopic motion has been demonstrated previously in nanoparticles [**Zhu2021**, **Rashid2018**, **Hoang2016**, **Kuhn2016**] but has not been observed for micron scale aggregates. What is interesting that the precession is seen around the particle's optical axis (in the case of a dimer this would be its long axis). Fig. 3.12 instead shows the precession occurring perpendicular to the optical axis. In the former case the precession was explained as simply occurring due to the reaction torque from the surrounding fluid [**Zhu2021**]. In their analysis of ellipsoidal particles, Zhu *et al.* found that when the particle rotated around their minimal inertial axis (similar to the observed behaviour in

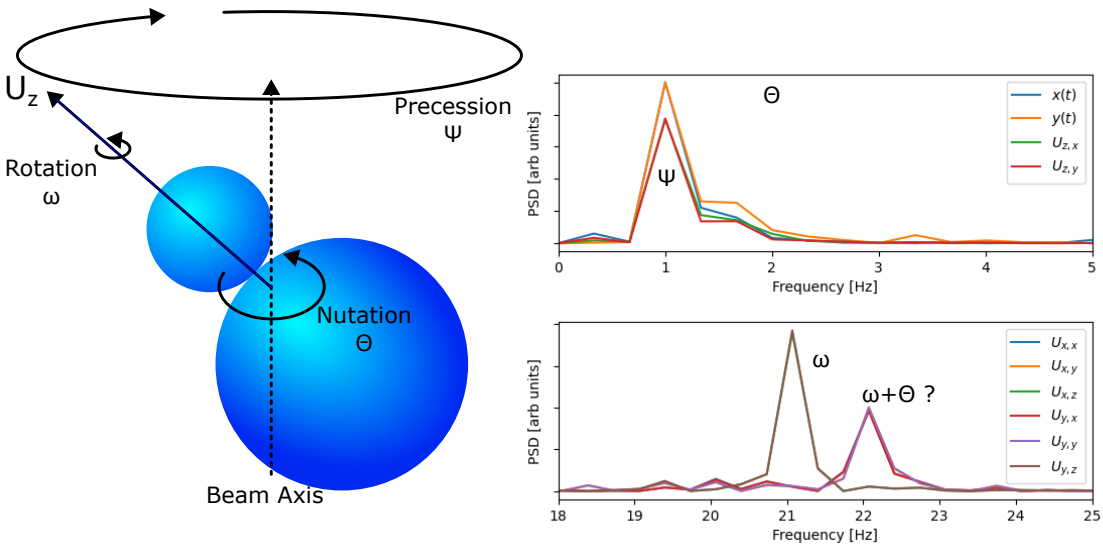

Figure 3.13: Representative diagram of the gyroscopic precession from fig. 3.12. The dimer has three principal angular frequencies: The rotation (ω) occurs around the the dimer's long axis. Precession (ψ) is seen where the dimer rotates around the beam axis. Nutation (θ) is due to the dimer's centre of diffusion orbiting the beam axis. Shown on the right is the power spectra from fig. 3.12 with the associated frequencies labelled. The power spectrum have been zoomed in on the relevant frequencies to highlight the precise values.

dimers), the particle would quickly 'stabilise' by aligning its' optical axis with the beam axis. This highlights that a spherical dimer is capable of rotating about its minimal inertial axis while remaining stably trapped. This has potential implications beyond simply understanding particle dynamics.

Further analysis of the mechanism behind the precession of off-axis dimers may provide insights into controlling Brownian motion. An experimental work trying to 'cool' nano-dimers by controlling the motion in all 6 degrees of freedom found that even while the rotation about the short axis' could be controlled the free rotation around the dimers' long axis resulted in an unpredictable torsional vibration [**Bang2020**]. Understanding how rotational motion arises in the Mie-regime could allow researchers to build a robust theoretical framework to construct beam structures that eliminate any unwanted rotational motion from a target particle. Conversely, the same framework could allow for precise measurements of the optical torque applied to a target particle, allowing for characterisation of complex shaped particles' interactions with an optical

trap.

3.6 Conclusions

Considering the simplicity of a scatterer such as a dimer, one would assume that the dynamics of such an object would be relatively easy to predict. Simulations of dimers in the Mie regime show that not only do they have multiple positions and orientations in which they can be trapped but also that their interaction with circularly polarised light is heavily dependent on the axial position and trapping orientation.

Dimer's have the potential to be used as tunable micro-rotors, being simple to synthesise and can be made out of any material of choice. The rotation demonstrated by dimer's is not accurately described in previous literature which raises questions on the interactions between circularly polarised light and spherical aggregates. Until now, our understanding of angular momentum transfer has been either focused on single particles (where momentum transfer is easily described by Lorenz-Mie theory) or for large aggregates of particles, where the angular momentum transfer between individual particles is not considered. This could provide a greater understanding of angular momentum and help in the development of better torque sensing or torque preventing methods.